Stochastic description of single nucleosome repositioning by ACF remodelers

Yves Vandecan and Ralf Blossey

Interdisciplinary Research Institute, USR 3078 CNRS and Université de Sciences et de Technologies de Lille, Parc de la Haute Borne, 50 Avenue de Halley, 59658 Villeneuve d'Ascq, France

(Received 22 March 2012; revised manuscript received 29 May 2012; published 22 June 2012)

Chromatin remodeling plays a crucial role in the activation or repression of transcription of eukaryotic genes. The chromatin remodeler ACF acts as a dimeric, processive motor to evenly space nucleosomes, favoring repression of gene transcription. Single-molecule experiments have established that ACF moves the nucleosome more efficiently towards the longer flanking DNA than towards the shorter flanking DNA, thereby centering an initially ill-positioned nucleosome on DNA substrates. In this paper we present a one-motor model with nucleosomal repositioning rates dependent on the DNA flanking length. The corresponding master equation is solved analytically with experimentally relevant parameter values. The velocity profile and the effective diffusion constant for nucleosome sliding, computed from the probability distributions, are in accordance with available experimental data. In order to address the observed kinetic pauses in experimental Förster Resonance Energy Transfer profiles, we extend the master equation to account for transitions between explicit motor states, i.e., adenosine triphosphate (ATP) loading and ATP hydrolysis in both ACF motors. The results of this extended two-motor model are compared to the previous effective one-motor model and allow insights into the role of the synchronization of the two motors acting on the nucleosome.

DOI: 10.1103/PhysRevE.85.061920 PACS number(s): 87.14.gk, 87.15.A−, 87.16.Nn

I. INTRODUCTION

Chromatin remodeling is the modification of the chromatin structure due to the repositioning or removal of nucleosomes [1]. Nucleosomal repositioning can be spontaneous due to thermal fluctuations or forced by adenosine triphosphate (ATP) dependent remodelers [2,3]. The latter are protein complexes with multiple functionalities; their key unit is a helicase-like ATPase derived from the superfamily SF2 of helicases. The functional subdivision of the remodeler families is based on the domains neighboring the ATPase domain, which allows us to distinguish four families: the *switching defective/sucrose nonfermenting* (SWI/SNF) family, which recognizes histone tail acetylations with the help of bromodomains; the *chromodomain, helicase, DNA binding* (CHD) family, which carries chromodomains to recognize histone tail methylations; the *inositol requiring 80* (INO80) family; and, of our concern here, the *imitation switch* (ISWI) family.

In this paper, we are concerned with the chromatin remodeler ACF, which is the abbreviation for *ATP-utilizing chromatin assembly and remodeling factor*, which belongs to the ISWI family of ATP-dependent chromatin-remodeling complexes [1]. A sketch of this dimeric remodeler is shown in Fig. 1. A major yeast homolog of ACF is ISW2, a complex which has three recognition sites in the remodeler-nucleosome complex. The first is the DEXD (ATPase) domain, which is given by the amino acid sequence from 180 to 376 and contains an aspartic acid (D)–glutamate (E) motif (X is any amino acid, and D is glutamate). It contacts DNA at 17–18 base pairs (bp) from the dyad axis; the two other domains are called the HAND domain (amino acid sequence from 745 to 882), which makes contacts at 60–62 bp, and, finally, the so-called SANT/SLIDE domain (amino acid sequences from 882 to 941 and from 977 to 1069, respectively), making contact at 92 bp [4]. These motor proteins have thus, in addition to the ATPase domain DEXD, two other recognition domains which bind to nucleosomal and extranucleosomal DNA. Hydrolysis of ATP induces conformational changes in the remodeler which pull the extranucleosomal DNA into the nucleosome, generating loops [5,6]. Unidirectional diffusion of the loop consequently repositions the nucleosome [7,8]. Concerning ACF, recent research has shown that it acts as a dimeric, processive motor by which nucleosomes are center positioned with respect to DNA strands [5,9–12]. *In vivo*, ACF, like other ISWIs, thus represses the transcription of genes by favoring the formation of regularly positioned nucleosomal arrays [13–15]. The catalytic subunits SNF2h of *human* ACF (hACF) that contact the nucleosome at opposing ends, i.e., the binding of the ATPase domains of SNF2h at the superhelix location (SHL) 2 (−2) located 17–18 bp (−17, −18 bp) from the dyad axis, are explicitly visualized in cryoelectron microscopy studies [10]. Electron paramagnetic spin resonance studies show that in the (unloaded) apo and the ADP states one of the two H4 tails is bound by one catalytic subunit SNF2h of hACF. The latter study combined with the fact that, in the apo and ADP states, the Hill coefficient takes a value of ≈2, thus indicating cooperativity, for the measured Cy3 fluorescence intensity (depending on the binding of SNF2h to the nucleosome) as a function of the SNF2h concentration, leads to the picture that one motor is attached to SHL 2 or −2, while the other motor serves as an anchor to stabilize the complex. The superhelix location refers to the position of the major groove of the DNA contacting the nucleosome counted from the dyad axis (SHL 0) in forward and backward directions, up to ±7.

Initiation of remodeling by hACF. Initiation of remodeling has recently been proposed to occur via a kinetic proofreading scheme [12,16,17]. Generally, kinetic proofreading scenarios play a role in molecular recognition systems to achieve high precision [18,19]. For ISWI/ACF, such a scenario has been put forward by Narlikar [12] based on single-molecule experiments in her group [9,11]. After binding of the ACF remodeler to the nucleosome [11], an ATP-dependent step appears before

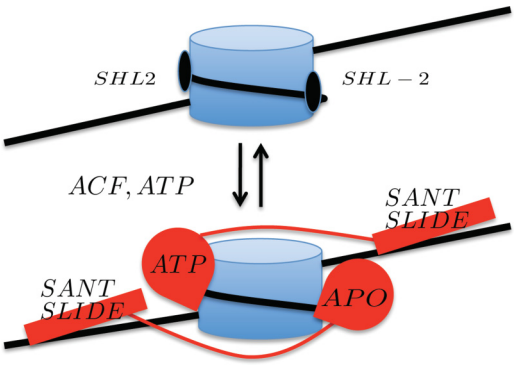

FIG. 1. (Color online) Schematic representation of the ACF remodeler, which acts as a dimeric motor. Each motor consists of an ATPase domain which binds ATP and a SANT-SLIDE domain which contacts extranucleosomal DNA. One motor loads ATP while the other motor remains in the (unloaded) apo state. The ATP-carrying motor binds the nucleosome tightly, and the second motor, weakly bound, serves as an anchor [5,10]. Communication between the two motors is required for a proper chromatin remodeling process. SHL indicates the approximate location of the binding site with respect to the histone octamer; see the text.

the actual remodeling of the nucleosome starts [11,12]. The recognition step involving binding to the unacetylated histone H4 tail and subsequent hydrolysis of ATP lead to an activation step according to the kinetic proofreading scheme [12,16] in chromatin remodeling by ISWI/ACF. Taking into account a second recognition step involving extranucleosomal DNA, an additional kinetic proofreading step is proposed to occur in ISWI/ACF remodeling [17].

Actual remodeling by hACF. Concerning the known experimental details of the actual remodeling by hACF, we consider gel mobility shift and Förster Resonance Energy Transfer (FRET) experiments to be important. Gel mobility shift experiments point to the existence of intermediates rather than continuous nucleosome remodeling towards the center of the DNA strand [9]. The gel electrophoretic mobility indicates that the intermediates differ 13 bp in linker length, i.e., $0N78, 13N65, \ldots$ The lNm state represents l bp linker DNA on the "left" side (entry site) and m linker DNA on the "right" side (exit site).

The actual remodeling dynamics are based on FRET experiments that translate the energy transfer between the donor dye on the DNA sequence and the acceptor dye on the H4 tail of the nucleosome into a proper value of the DNA linker length [9]. These experiments are used to determine the transition rates between the intermediates. Using nucleosomes with different flanking lengths, a plot of the natural log of the rate constant $\ln(k)$, proportional to the activation energy of the reaction, versus their DNA flanking length is a straight line up to 60 bp linker length [9]. The reason for this phenomenon is that there appears an optimal range in which the remodeler can operate due to the concerted action between the ATPase unit, located at SHL-2 or SHL2, and the SANT-SLIDE domain that contacts the extranucleosomal DNA [20]. In this optimal range, from 60 up to 100 bp, the activation energy no longer changes with the linker length.

The FRET time traces further reveal kinetic pauses during active remodeling [11], possibly related to ATP binding events. The FRET time traces show kinetic steps, or translocation steps, of 7 bp, 3 bp, and again 3 bp between the kinetic pauses, summing up to the 13 bp translocation per ATP hydrolysis event in the case of ACF, and therefore they are consistent with the experimentally observed intermediates $0N78, 13N65, \ldots$ in gel mobility shift experiments. It is important to note that, experimentally, the kinetic steps, as well as the kinetic pauses, depend on the ATP concentration [11]. The experimental systems considered here are a gel mobility shift experiment with 10 μM ATP and a FRET experiment with 2 μM ATP [9,11]. The ACF concentrations are 25 and 6 nM, respectively.

Our approach. In this paper we address the motor action of the chromatin remodeler ACF and its capability of positioning a single nucleosome. We introduce two models: a single-motor model and a two-motor model. This allows us to build different levels of detail into the description. In the one-motor model, we use experimental information from gel mobility shift and FRET experiments to predict velocity profiles, effective diffusion constants, and the probabilities of the intermediates. In the two-motor model, we additionally link the synchronization of the motors to the experimentally observed kinetic pauses of the remodeling complexes, which allows a more detailed analysis of the FRET time traces.

We first discuss a master equation of the one-motor model. Conformational changes between the ATPase and extranucleosomal DNA binding domain are expected to pull in linker DNA from either side (entry and exit sites), resulting in the idea that one motor is translocating to the left and the other to the right [5], although more experimental evidence is called for. This idea of the alternating action between the two ACF motors and the dependence of the ATP-hydrolysis rate on the DNA flanking length [20], which leads to a competition between back and forward movement of the nucleosome [5,9], is in this simple first model properly translated into the length dependence of the transition rates. We took the experimentally determined transition rates from [9,11]. Second, the communication between the two motors is considered using an extended master equation which models explicit motor states. The idea of ATP loading as a means to account for the observed kinetic pauses and sampling between the two motors consequently enters the description.

This paper is organized as follows: we start by writing down the master equation for the one- and two-motor models and give a solution method for these first-order partial differential equations. The computed motor velocity profiles and the effective diffusion constants for the two models are compared with experimental data. We finally discuss the effects of different parametrizations of the two-motor model.

II. TWO NUCLEOSOME REPOSITIONING MODELS

A. The effective one-motor model

As a starting point for our analysis we assume that a nucleosome in a solution can be in one of three states. The first state corresponds to a free nucleosome, not bound to the remodeler ($N + R$). In the second state, the nucleosome is bound to the remodeler, forming a nucleosome-remodeler complex (NR).

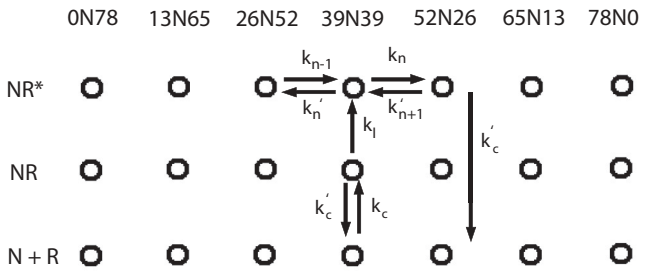

FIG. 2. The small circles of each row represent the nucleosomal intermediates with different extranucleosomal length ($n = 1, \ldots, 7$). The rows refer to $N + R$, NR, and NR^* (see text). The proper rates between the multiple states are indicated by arrows.

Finally, the third state refers to partially loosened DNA around the nucleosome due to the remodeler's consumption of one ATP (NR^*). In this loosened state, successive intermediates are generated by the successive movement of 13 ± 3 bp of DNA across the histone octamer, thereby consuming one ATP molecule per remodeling event [9].

More specifically, we consider a three-state model with seven different intermediates with respect to the DNA (see Fig. 2). The seven repositioned nucleosomes are ($0N78, 13N65, 26N52, 39N39, 52N26, 65N13$, and $78N0$; $n = 1, \ldots, 7$), as experimentally verified. We represent the on rate from $N + R$ to NR as k_c, the off rate from NR and NR^* to $N + R$ as k'_c, the rate from NR to NR^* as k_I (activation step), and the extranucleosomal DNA-dependent remodeling rates in the direction $n \to n + 1$ ($n \to n - 1$) as $k_n(k'_n)$. Further, if $P_k(n,t)$, $k = 1,2,3$, are respectively the probabilities of the nucleosome-remodeler complex occupying the states $N + R$, NR, and NR^*, with n referring to the position of the nucleosome along the DNA strand, then the master equation can be written as

$$\frac{\partial P_1(n,t)}{\partial t} = -k_c P_1(n,t) + k'_c P_2(n,t) + k'_c P_3(n,t), \quad (1)$$

$$\frac{\partial P_2(n,t)}{\partial t} = k_c P_1(n,t) - (k_I + k'_c) P_2(n,t), \quad (2)$$

$$\frac{\partial P_3(n,t)}{\partial t} = k_I P_2(n,t) - (k'_c + k'_n + k_n) P_3(n,t) + k_{n-1} P_3(n-1,t) + k'_{n+1} P_3(n+1,t). \quad (3)$$

Our three-state model with appropriate rates is schematically depicted in Fig. 2.

According to Michealis-Menten kinetics, we consider the following enzymatic reaction scheme for the DNA translocation step:

$$N_n R^* + \text{ATP} \rightleftharpoons N_n R^* - \text{ATP} \to N_{n\pm1} R^* + \text{ADP} + P.$$

Here $N_n R^*$ represents the nucleosome-remodeler complex, where the nucleosome is in the loosened intermediate state n without ATP bound, and $N_n R^* - \text{ATP}$ reflects the same complex with ATP bound. The reaction rate r of the formation of the product [21], here the remodeling step, is given by

$$r = V_{\max} \frac{[\text{ATP}]}{[\text{ATP}] + K_m}, \quad (4)$$

TABLE I. The computed values of the model parameter k_0 as a function of the ATP concentration.

[ATP] (μM)	k_0 (min^{-1})
2	0.013
10	0.057
20	0.098
200	0.27
2000	0.33

where $V_{\max}$ is the maximal speed of the reaction, [ATP] is the ATP concentration, and K_m is the Michaelis constant [22].

Using the Arrhenius equation, the maximal reaction speed $V_{\max}$ is proportional to $e^{-E_a/kT}$, where E_a is the activation energy. If the remodeler concentration is saturated, then this concentration must not be taken into account. As explained in the Introduction, experiments reveal that the activation energy varies linearly with the DNA flanking length up to 60 bp for ACF. As a consequence, the transition rates are linker length dependent too. From 60 up to $\approx$100 bp, the transition rates are assumed to be constant but are expected to decrease to zero at a DNA flanking length of $\approx$160 bp [20] due to loss of contact of the DEXD domain at the SHL-2 or SHL2 location (see Fig. 1 and [20]). The same accounts for values of the DNA flanking length lower than 20 bp. Analytically, the transition rate dependence takes then the following form:

$$k_n = \begin{cases} 0, & 0 < \ell < \ell_{\min}, \\ k_0 e^{a\ell}, & \ell_{\min} \leqslant \ell \leqslant \ell_{\max}, \\ k_0 e^{a\ell_{\max}}, & \ell_{\max} < \ell \leqslant \ell_c\,. \end{cases} \quad (5)$$

The experimentally estimated parameter values for an ATP concentration of 10 μM (gel mobility shift experiment) are $k_0 = 0.057/\text{min}$, $a = 0.077\,\text{bp}^{-1}$, $\ell_{\min} = 20\,\text{bp}$, $\ell_{\max} = 60\,\text{bp}$ and $\ell_c = 100$ bp. Concerning the remaining rates for an ATP concentration of 10 μM, we choose $k_c = 12/\text{min}$, $k'_c = 8/\text{min}$, and $k_I = 27/\text{min}$ (see [11,12] and Table II).

From the experimental data of the gel mobility shift experiment, Eq. (4) allows us to compute k_n for different ATP concentrations. It suffices to calculate $k_0([\text{ATP}])$ (see Table I) because the parameter a is independent of the ATP concentration. The Michealis-Menten constant is taken to be 50 μM, according to the previous experiment.

The master equation is a system of coupled linear partial differential equations of first order which can be written in the form

$$\frac{d}{dt}\vec{P} = \mathbf{M}\vec{P}, \quad (6)$$

where $\vec{P} = [P_k(n,t)]^{\mathrm{T}}$, with $(k,n) = (3,7)$ being a (21×1) vector and $\mathbf{M}$ being a (21×21) rate matrix for $n = 7$. Substitution of $\vec{P} = \mathbf{C}\vec{P}_N$ in Eq. (6), with $\mathbf{C}$ being the invertible matrix of eigenvectors of $\mathbf{M}$, transforms the system into a set of uncoupled linear partial differential equations, i.e.,

$$\frac{d}{dt}\vec{P}_N = \mathbf{D}\vec{P}_N, \quad (7)$$

where $\mathbf{D}$ is the diagonal matrix of eigenvalues λ_i for $i = k \cdot n = 1, \ldots, 21$ and $\vec{P}_N$ is the vector of normal modes. The general solution is then obtained in terms of a linear combination of normal modes,

$$P_i(t) = \sum_{j=1}^{N_o} u_{ij} c_j e^{\lambda_j t}, \tag{8}$$

where $P_i(t)$ is component i of vector $\vec{P}$, N_o is the length of vector $\vec{P}$, u_{ij} are the components of matrix $\mathbf{C}$, and c_j are the constants referring to the initial condition.

B. The two-motor model

The effective translocation steps with rate k_n (k_n') in Fig. 2 consist of translocation and ATP-loading steps. In order to investigate the separate effects of these steps, we split the previous nucleosome-remodeler state NR^* ($0N78$, $13N65, \ldots$) into four explicit motor states, i.e., (ATP, 0), (ADP, 0), (0, ATP), and (0, ADP). The (ATP, 0) and (ADP, 0) states reflect that the adenosine triphosphate and adenosine diphosphate are bound at the ATPase unit of motor 1 while the other motor is in the apo state (unloaded state) and vice versa for the other two states. We presume that the two motors translocate DNA in opposite directions. Considering transitions between these different motor states, we let the motors communicate among each other (see Fig. 3).

Hydrolysis of ATP (ATP $\rightarrow$ ADP) with the subsequent translocation step is depicted by large black arrows in Fig. 3 labeled with rate k_n or k_n'. We clearly see that the ATP hydrolysis at the ATPase unit of motor 1 translocates in the opposite direction compared to motor 2. In order to include the dependence of the rate of ATP hydrolysis with subsequent translocation steps on the extranucleosomal DNA length, we assume once again Eq. (5), but with a modified k_0 value. The parameter a reflects the intrinsic flanking-length dependence and should be unchanged.

The dark gray arrows with rate k_p refer to the ATP-loading phase, i.e., the dissociation of ADP with the binding of a new ATP molecule to the ATPase unit of motor 1 or 2. We include also transitions between (ATP, 0) and (0, ATP) [blue (light gray) arrows with rate k_u], which represent unbinding of a nonhydrolyzed ATP molecule belonging to the ATPase unit of motor 1 (2) and subsequent binding of an ATP molecule at the ATPase unit of motor 2 (1). These stages reflect ATP loading, presumably related to the kinetic pausing of the remodeler.

In view of a highly processive motor (with a low k_c' value) and to gain insight into the effects of ATP loading and translocation separately, it suffices to restrict our description to the active remodeling phase together with the $N + R$ and NR states of the end-positioned nucleosome $0N78$ (see Fig. 3). Because we neglect the dissociation of the remodeler in the NR^* states, the $N + R$ and NR states of the $0N78$ state will only induce a time delay. These assumptions reduce the number of possible states (28 states). The extended master equation then reads:

$$\frac{\partial P_1(t)}{\partial t} = -k_c P_1(t) + k_c' P_2(t), \tag{9}$$

$$\frac{\partial P_2(t)}{\partial t} = k_c P_1(t) - (k_I + k_c') P_2(t), \tag{10}$$

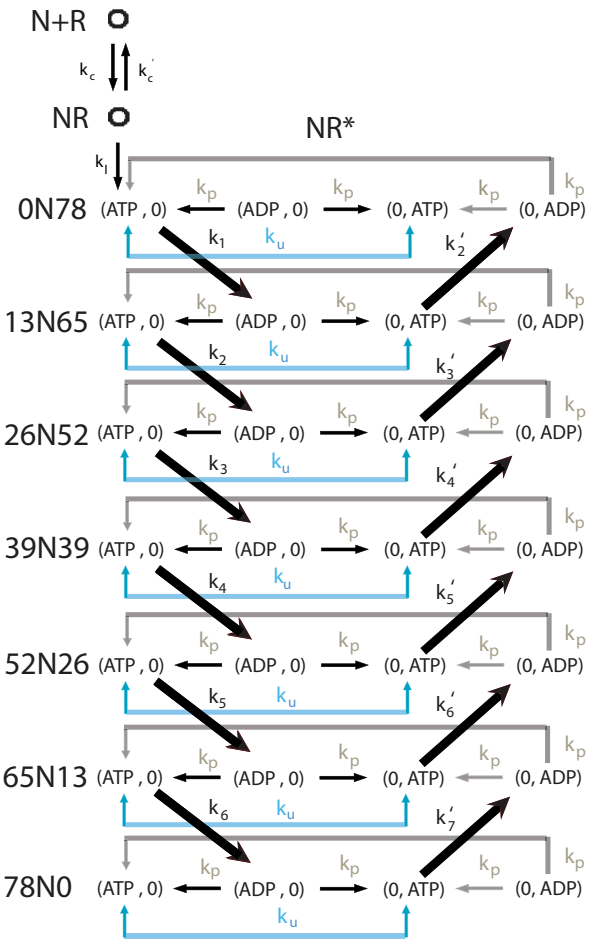

FIG. 3. (Color online) The presumed motor states (1, 2) of the dimeric ACF remodeler with the transitions among them. The big black arrows denoted by k_n and k_n' reflect the translocation step using ATP hydrolysis, i.e., the transition from the (ATP, 0) to (ADP, 0) state for motor 1. The same is shown for motor 2, but with the reverse translocation step. The ATP-loading step is split into two distinct transitions. The first type of transition is the arrows with rate k_p (black and dark gray), which represent the reloading from an ADP to an ATP state after the translocation step. The second type is depicted by arrows with rate k_u [blue (light gray)], which reflect the unbinding of the ATP molecule at motor 1 and binding of an ATP molecule to motor 2 or vice versa.

$$\frac{\partial P_3(n,1,t)}{\partial t} = -(k_n + k_u) P_3(n,1,t) + k_p [P_3(n,2,t) + P_3(n,4,t)] + k_u P_3(n,3,t) + k_I P_2(t) \delta_{n,1}, \tag{11}$$

$$\frac{\partial P_3(n,2,t)}{\partial t} = -2k_p P_3(n,2,t) + k_{n-1} P_3(n-1,1,t) \quad (n \neq 1), \tag{12}$$

$$\frac{\partial P_3(n,3,t)}{\partial t} = -(k_n' + k_u) P_3(n,3,t) + k_p [P_3(n,2,t) + P_3(n,4,t)] + k_u P_3(n,1,t), \tag{13}$$

$$\frac{\partial P_3(n,4,t)}{\partial t} = -2k_p P_3(n,4,t) + k'_{n+1} P_3(n+1,4,t) \quad (n \neq 7), \qquad (14)$$

with the initial condition $P_1(t=0)=1$. $P_1(t)$ and $P_2(t)$ represent the $N+R$ and the NR states of the end-positioned nucleosome, respectively. $P_3(n,M,t)$ reflects the loosened state NR^*, with $n=1,\ldots,7$ being the previously discussed intermediates and $M=1,\ldots,4$ being the four motor states, i.e., (ATP, 0), (ADP, 0), (0, ATP) and (0, ADP), in that order. Here $\delta_{n,1}=1$ when $n=1$ and 0 otherwise. Furthermore, $P_3(1,2,t)=P_3(7,4,t)=0$ due to the initial condition $P_1(t=0)=1$. The extended master equation will be solved with the same mathematical technique as discussed above.

III. RESULTS AND DISCUSSION

A. The effective one-motor model

In order to examine the remodeling process, we consider the mononucleosomes initially in one of the seven free nucleosome states with different flanking DNA lengths, i.e., $0N78$, $13N65$, $26N52$, $39N39$, $52N26$, $65N13$, and $78N0$. In the vector $\vec{P}$, this corresponds to setting the component $P(n,t=0)=1$ for each $n \in \{1,\ldots,7\}$ and $P(m,t=0)=0$ otherwise for the remaining $m \neq n$. The time evolution of the probability distribution $P(n,t)$ is shown in Fig. 4. Irrespective of the initial condition (only $0N78$ and $13N65$ are shown in Fig. 4), the steady-state probability of $P(n=4,t)$ ($39N39$) reaches nearly 60%, indicating that the remodeler produces mainly center-positioned nucleosomes in all cases, as experimentally observed [11,20]. The transition times to reach the steady-state condition obviously depend on the on rate k_c, off rate k'_c, and the activation step rate k_1.

During the remodeling process, the motor velocity v along the DNA chain is computed from

$$v = \frac{d}{dt}\left(\sum_{n=1}^{7} P(n,t)x_n\right). \qquad (15)$$

Here, x_n is the nucleosome-remodeler position with respect to the DNA. The distance $x_n = 0,13,\ldots$ reflects the $0N78$, $13N65,\ldots$ state. For end-positioned nucleosomes ($0N78$ and $78N0$), the nucleosome sliding velocity reaches a maximum of ≈0.5 bp/s at $t \approx 20$ s (at an ATP concentration of 10 μM) to converge to zero velocity when the nucleosome is center positioned with respect to the DNA chain [see Fig. 5(a)]. The steady-state velocity for $t \to \infty$ is therefore zero [23]. An initially centered nucleosome stays, of course, in the center and has no sliding velocity. The repositioning time from an end-positioned nucleosome $0N78$ to a nearly completely remodeled state ($37N41$, 37 bp flanking DNA, i.e., 95% of 39 bp) of 200 s is in good agreement with the gel mobility shift experiment [9], although it is a little bit slower. This effective one-motor model is merely an extension (with a binding step and an activation step) of the model proposed in the gel mobility shift experiment. Concerning the FRET experiment at 2 μM ATP, we obtain an average velocity of ≈0.005 bp/s, according to the previous 95% of 39 bp definition. Once more, this theoretical result is clearly slower than the experimental value of ≈0.05–0.1 bp/s [11].

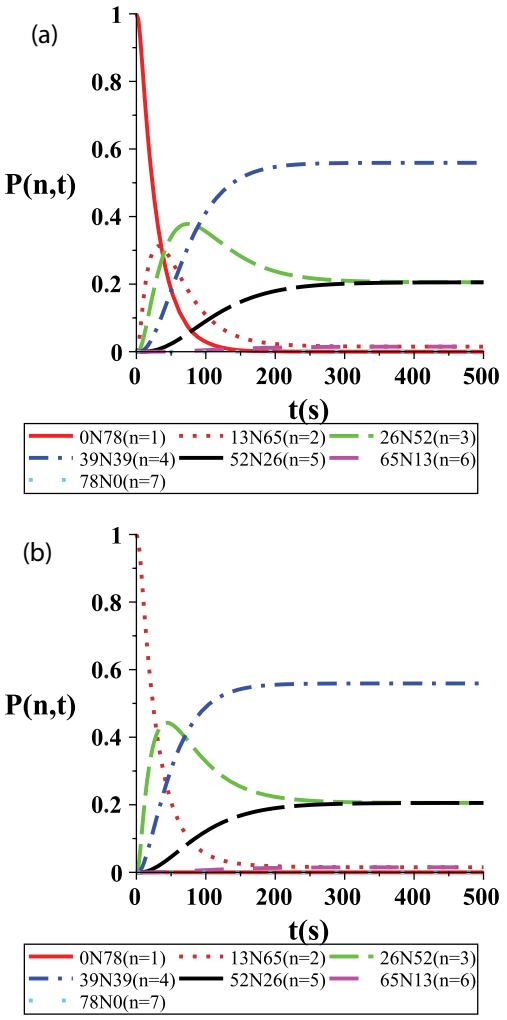

FIG. 4. (Color online) The probability distribution $P(n,t)$ of the effective one-motor model finding the mononucleosome in repositioned state n after time t, with the initial conditions (a) $0N78$ and (b) $13N65$. The ATP concentration is in both cases equal to 10 μM ATP.

Comparing the upper limit of 8/min [12] for k'_c to the 5/min for the initial translocation steps k_1 and k_2 leads to the prediction that the ACF motor will fall off before complete remodeling, as experimentally observed in a chase experiment [9]. On the contrary, more recent experiments [11] point to a highly processive motor, i.e., a motor capable of finishing the complete remodeling before falling off. Lowering k'_c to 1/min, which improves the processivity of the motor, increases, at 2 μM ATP, the average velocity from ≈0.005 to ≈0.05 bp/s. The repositioning time decreases from ≈200 to ≈100 s in the case of 10 μM ATP. Consequently, lowering the value of the off rate k'_c to 1/min clearly improves the agreement with experiments.

The effective diffusion constant [24]

$$D_{\text{eff}} = \left[\sum_{n=1}^{7} P(n,t)x_n^2 - \left(\sum_{n=1}^{7} P(n,t)x_n\right)^2\right] \Big/ (2t) \qquad (16)$$

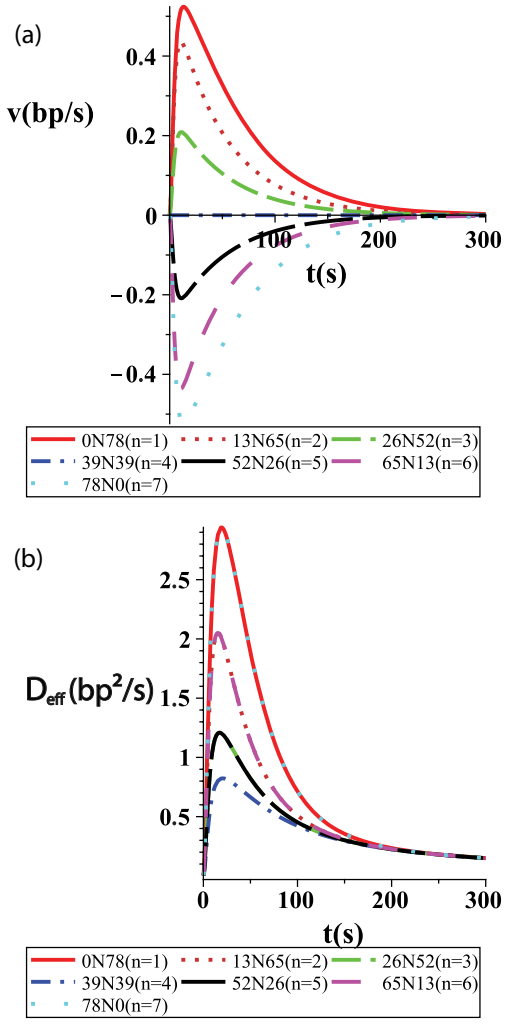

FIG. 5. (Color online) (a) The motor velocity, or the nucleosome sliding velocity, for the effective one-motor model. The nucleosome sliding velocity reaches a maximum at $t \approx 10$ s and decreases to zero velocity when the nucleosome is center repositioned with respect to the DNA. (b) The effective diffusion constant for the different initial positions. The ATP concentration is in both cases equal to 10 μM ATP.

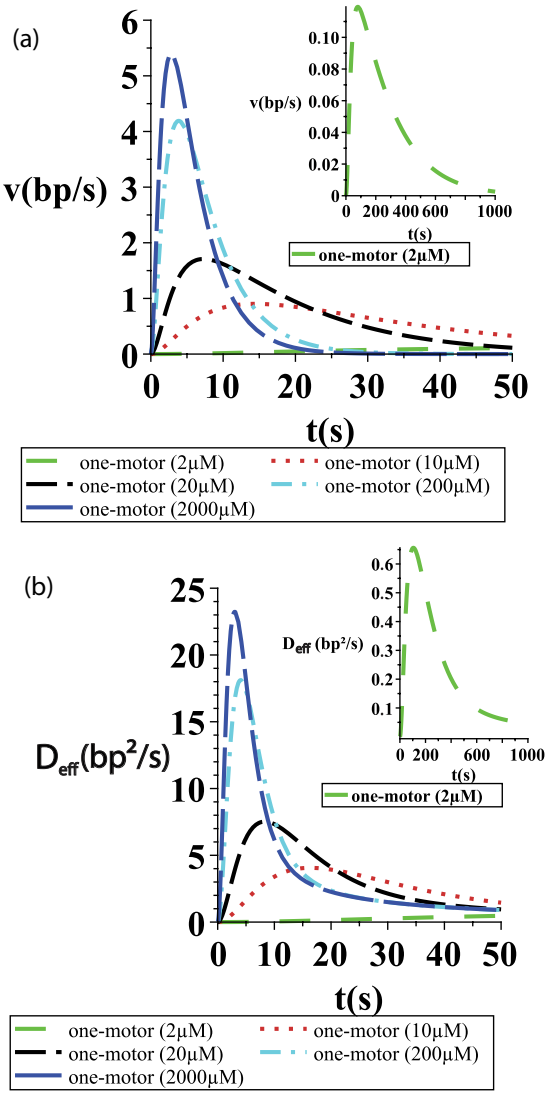

FIG. 6. (Color online) (a) The motor velocity, or nucleosome sliding velocity, for the effective one-motor model with an initially end-positioned $0N78$ nucleosome (and $k_c' = 1/\text{min}$) at different ATP concentrations. The nucleosome sliding velocity reaches a maximum at $t \approx 10s$ to decrease to zero velocity, when the nucleosome is center repositioned with respect to the DNA. (b) The corresponding effective diffusion constants for the one-motor model at different ATP concentrations.

reaches a maximal value of 1–2 bp^2/s [see Fig. 5(b)]. We introduce the Péclet number as a measure of linear transport compared to diffusion,

$$\text{Pe} = \frac{v\ell}{D_{\text{eff}}}. \tag{17}$$

Here, v is the expected velocity, as defined in Eq. (15), and ℓ is a characteristic length scale of the system. In our model the Péclet number reaches zero for the time $t \to \infty$, indicating that the velocity profiles decrease more rapidly to zero than the effective diffusion constant. Large position fluctuations can then be expected at steady state, which are indeed observed in the experimental FRET studies [11] due to the bidirectional and processive movement of ACF.

Finally, for comparison with the extended two-motor model in the next section, we restrict our calculation for different ATP-concentrations to the initial condition $0N78$ and set $k_c' = 1/\text{min}$ (high processivity), using the values of Table I. The computed velocity profiles and the effective diffusion constant are shown in Fig. 6.

B. Two-motor model

We focus now on the extended two-motor model (see Fig. 3). The model rates k_u, k_p, and k_n are related to the experimental kinetic pauses (assuming that the kinetic pauses reflect ATP-loading time) and translocation steps [11]. We recall $k_n = k_0 e^{a\ell}$ [Eq. (5)], as already mentioned, with the intrinsic length dependence $a = 0.077$ bp^{-1} and assume the same binding and unbinding rate of ATP and ADP, i.e., $k_u = k_p$.

Concerning the translocation steps, we let the 13 bp intermediates in our model correspond to the sum of the kinetic steps of 7 bp, 3 bp, and again 3 bp (between kinetic pauses), experimentally observed in the initial remodeling of the $0N78$ ($n = 1$) nucleosome [11]. The step time τ_{tr} per intermediate is consequently a simple summation of the individual ATP-dependent kinetic step times, and $k_1 = 1/\tau_{tr}$. The parameter k_0, independent of the DNA flanking length, can then be determined for all intermediates.

Concerning the kinetic pauses, we presume an effective pause τ_k, representing the ATP-loading step, as a sum of the experimentally observed first, second, and third kinetic pauses [11]. In the motor state (ADP, 0) (of the intermediate $13N65$), we expect a 50% chance to make the direct transition (ADP, 0) $\rightarrow$ (ATP, 0) and a 50% chance to make the transition (ADP, 0) $\rightarrow$ (0, ATP), followed by the sampling step (0, ATP) $\rightarrow$ (ATP, 0). This yields the expression

$$\frac{3}{2}\frac{1}{k_p} = \tau_k, \tag{18}$$

which links the effective pause τ_k to the internal motor state transitions k_p and k_u. As a consequence, we have k_p and k_u for all the intermediates. The values of k_u, k_p, and k_0 used for several ATP concentrations, as well as the values of the on rate k_c and the activation step k_I, which are both ATP dependent too, are given in Table II [11].

The typical probability density functions of the advanced two-motor model are similar to the simpler effective one-motor model at the same ATP concentration (see Figs. 4 and 7), although a broader distribution of intermediates is obtained from the two-motor model at steady state. From the probability density distributions, the velocity profiles and the effective diffusion constant as a function of the ATP concentration can again be calculated and are depicted in Fig. 8.

The maximal velocity increases from 0.1 to 5 bp/s as a function of augmenting ATP concentration (from 2 μM to 2 mM). While the one-motor model uses effective remodeling rates from normalized Cy3 intensities in FRET studies [9] and the two-motor model includes experimental kinetic pauses and translocation steps (thus analyzing the FRET time traces more in detail), these experimental results independently give

TABLE II. The estimated values of the model parameters k_0 and $k_p (= k_u)$ as a function of the ATP concentration. The sample values of $1/t_{\text{wait}}$ for 20, 200, and 2000 μM are estimated from [11], and we set $k_c = \frac{3}{2}(1/t_{\text{wait}})$ and $k_I = 3(1/t_{\text{wait}})$. The latter values are multiplied by a factor of 3 (in rough approximation) to obtain a system saturated in ACF. The waiting time t_{wait} for 2 μM is taken from more detailed waiting time distributions [11], which have an average of $\approx$50 s for a rather high ACF concentration of 16 nM. Concerning the values of k_0 and k_p, we estimated these values from the experimental graphs of [11].

[ATP] (μM)	k_0 (min^{-1})	k_p (s^{-1})	k_c (s^{-1})	k_I (s^{-1})
2	0.02	0.02	0.03	0.06
10	0.15	0.1	0.2	0.45
20	0.3	0.2	0.45	0.9
200	0.5	0.4	0.7	1.4
2000	0.6	0.6	1.0	2.1

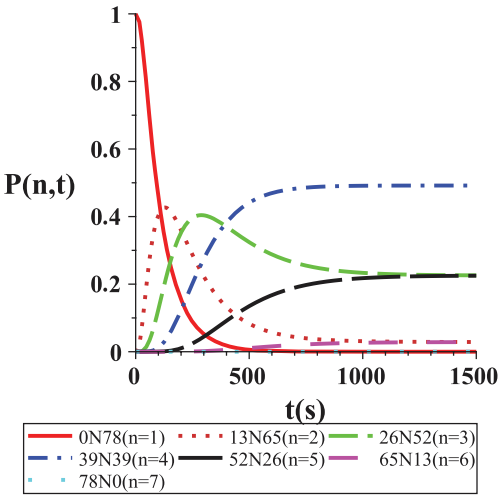

FIG. 7. (Color online) The probability density function of the intermediates as a function of time, computed from the advanced two-motor model and thus starting from an initially end-positioned $0N78$ nucleosome. The ATP concentration corresponds to 2 μM.

rise to qualitatively similar, acceptable velocity profiles and effective diffusion constants. We may therefore conclude that our assumptions in the two-motor model, describing a more detailed communication scheme between the two motors and explaining the phenomenon of kinetic pauses as ATP-loading periods, are reasonable.

Both models include an ATP-dependent binding step of ACF, as experimentally observed [11], which renders the description more realistic. It remains to be said that, at high ATP concentrations, the expected velocities of the effective one-motor model are quantitatively higher than those of the extended two-motor model. At low ATP concentrations (up to 20 μM ATP), these differences are negligible. The average velocity therefore, calculated according to the same definition as in the one-motor model, approximates 0.05 bp/s for a low ATP concentration of 2 μM (the long-space-dashed green bottom curve in the Fig. 8 or the only curve in the inset), which reflects rather well the obtained $\approx$0.05–0.1 bp/s remodeling speed, derived from the experimental FRET study at the same ATP concentration [11]. The same accounts for the gel mobility shift experiment at 10 μM ATP. In the ATP concentration interval from 2 μM to 2 mM, the effective diffusion constant ranges from 0.4 to 15 bp^2/s at the maximal remodeling velocity. Similar effective diffusion constants are obtained when comparing the one- and two-motor models at the same ATP concentration. However, at high ATP concentrations, like the velocity profiles, the effective diffusion constants of the one-motor model are quantitatively higher than those of the two-motor model.

An interesting point is that the blue (light gray) arrows with rate k_u (see Fig. 3), the unbinding of ATP from motor 1 and the binding of ATP to motor 2, reflect the sampling between the two motors [10]. Statistically, there is a 50% chance that the ATP molecule is bound to the wrong motor in view of centering the nucleosome with respect to DNA. However, the ATP-hydrolysis rate towards the short flanking DNA (e.g., transition rate $k_2' \approx 0.1$/min) is low enough that the

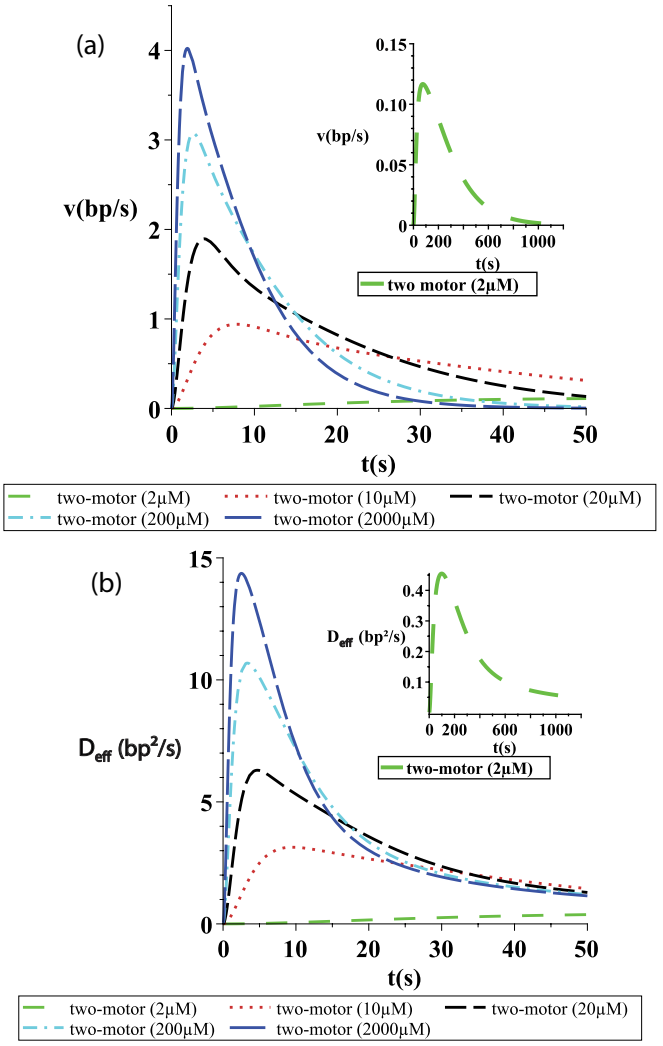

FIG. 8. (Color online) (a) The motor velocity, or the nucleosome sliding velocity, for the advanced two-motor model with an initially end-positioned $0N78$ nucleosome at different ATP concentrations. The nucleosome sliding velocity reaches a maximum at $t \approx 10$–20 s and decreases to zero velocity when the nucleosome is center repositioned with respect to the DNA. (b) The corresponding effective diffusion constants for the two-motor model at different ATP concentrations.

ATP molecule unbinds and binds to the ATPase unit of the other motor with a high probability. The ATP-hydrolysis rate of the motor towards the longer flanking DNA (e.g., transition rate $k_1 \approx 5$/min) is fast, so it is probable that the translocation step is actually done. Neglecting the blue (light gray) arrows with rate k_u or setting the corresponding transition rates to a very low value results in nucleosome-remodeler complexes which are not center positioned with the highest probability at steady state (see Fig. 9). Mathematically, we keep the rate k_p fixed (the same value as in Table II) and use the rate $k_u \to 0$ in the scheme of the two-motor model. Thus, this model emphasizes the fact that, after arriving at an ADP state, not only is the next ATP loading to the ATPase unit of either motor (the dark gray arrows with transition rates k_p) important, but a subsequent sampling by binding and unbinding ATP molecules between

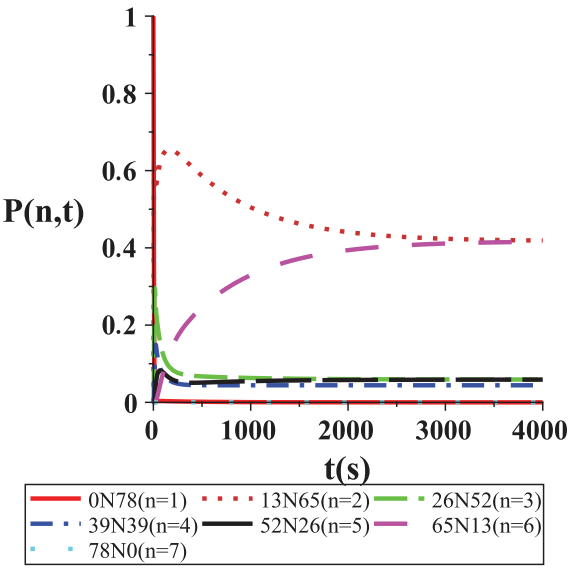

FIG. 9. (Color online) When the sampling between the two motors is turned off (the value of k_u is reduced by a factor of 100), the probability density function of the advanced two-motor model does not produce center-positioned nucleosomes with the highest probability at steady state. The ATP concentration corresponds to 20 μM.

the ATPase units of the motors [blue (light gray) arrows with transition rate k_u] is required too.

C. Further insights from a different model parametrization

More rigorous computations of the on rate k_c and of the activation step rate k_I reveal interesting insights about the processivity of the ACF motor and the robustness of both models. According to Michealis-Menten kinetics of the ACF binding followed by an ATP-dependent activation step, the inverse of the waiting time $1/t_{\text{wait}}$ is then given by

$$1/t_{\text{wait}} = \alpha(\text{ATP}) \frac{[\text{ACF}]}{[\text{ACF}] + K_{\text{ACF}}} \frac{[\text{ATP}]}{[\text{ATP}] + K_{\text{ATP}}}. \quad (19)$$

After curve fitting of this formula with experimental data points [11], $K_{\text{ACF}} \approx 4.8\,\mu$M and $K_{\text{ATP}} \approx 117\,\mu$M. The proportionality constant $\alpha \approx 0.7\ \text{s}^{-1}$ for the high concentrations of [ATP] $= 200$ and $2000\ \mu$M. For low ATP concentrations $\alpha \approx 0.56$ with [ATP] $= 20\ \mu$M and $\alpha \approx 1.3$ with [ATP] $= 2\mu$M. These minor deviations in α are due to the fact that K_{ACF} is ATP dependent too (an ATP-dependent ACF binding step), but we lack the experimental data for the ATP dependence of K_{ACF}.

The activation step rate $k_I = 1/\langle t_{\text{lag}} \rangle$ with the average lag time $\langle t_{\text{lag}} \rangle$ and the binding rate $k_c = 1/\langle t_{\text{bind}} \rangle$ with the average binding time $\langle t_{\text{bind}} \rangle$ are calculated from the waiting-time distributions of the experimental systems for [ACF] $= 4$ nM and [ATP] $= 2$ and $20\ \mu$M [11]. The lag time is only ATP dependent, and the values for high ATP concentrations are predicted by

$$1/\langle t_{\text{lag}} \rangle = A \frac{[\text{ATP}]}{[\text{ATP}] + K_{\text{ATP}}}, \quad (20)$$

TABLE III. The model parameters $k_c = 1/\langle t_{\rm bind}\rangle$ and $k_I = 1/\langle t_{\rm lag}\rangle$ as a function of the ATP concentration, with [ACF] = 4 nM and a saturated system of [ACF] = 30 nM from more rigorous approximations.

[ATP]	k_c (s^{-1})		k_I
(μM)	[ACF] = 4 nM	[ACF] = 30 nM	(s^{-1})
2	0.024	0.1	0.023
20	0.06	0.26	0.1
200	0.36	2.7	0.44
2000	0.55	3.9	0.66

with a fitted value of $A \approx 0.7\ s^{-1}$. Because the waiting time is the sum of the binding and the lag times, i.e., $t_{\rm wait} = t_{\rm lag} + t_{\rm bind}$, Eq. (19) permits the computation of $k_c = 1/\langle t_{\rm bind}\rangle$. All values are gathered in Table III.

Concerning the effective one-motor model, in the case of our referred experimental systems, these more rigorous k_c and k_I approximations show once again that the k_c' upper limit of 8/min is too high and point to a highly processive motor with k_c' values even lower than 1/min. A high processivity supports our two-motor model, which does not include the dissociation of the remodeler while actively translocating. Nevertheless, the velocity profiles with the more rigorous calculations of k_c and k_I are qualitatively similar to profiles generated with the rough approximations of k_c and k_I (see Fig. 10), which emphasizes the robustness of the advanced two-motor model against model parameter estimations. Quantitatively, however, these velocity profiles are lower compared to the case of the rough approximations for k_c and k_I.

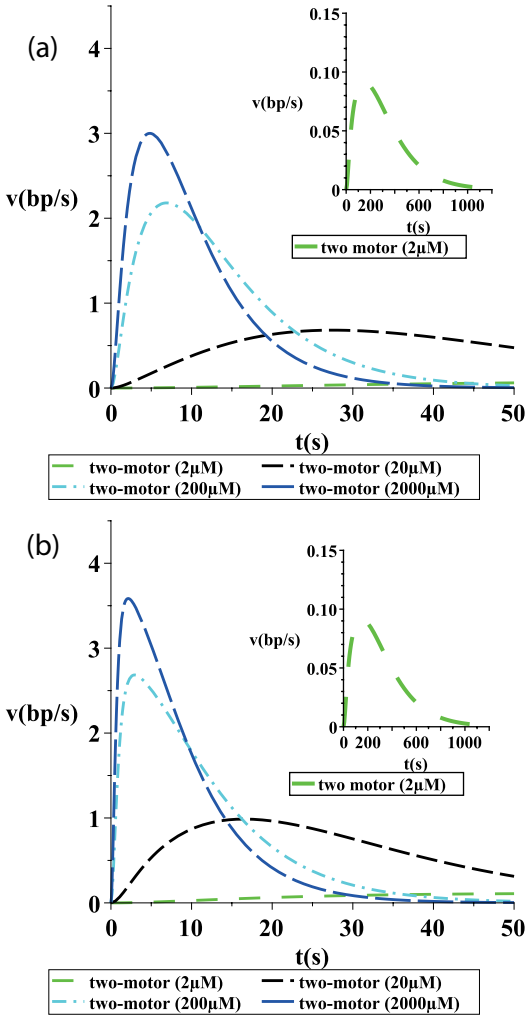

FIG. 10. (Color online) The motor velocity, or the nucleosome sliding velocity, for the advanced two-motor model with an initially end-positioned $0N78$ nucleosome at different ATP concentrations, using Table III, with (a) [ACF] = 4 nM and (b) [ACF] = 30 nM.

IV. CONCLUSION

We solved analytically a master equation of an effective one-motor model for the repositioning of a single nucleosome, motivated by recent gel mobility shift and FRET experiments [10,12]. After adding ACF and ATP to the nucleosomes, this model predicts that the end-positioned nucleosomes reach a maximal sliding velocity of 0.5 bp/s for an ATP concentration of 10 μM. Starting from an end-positioned nucleosome, a repositioning time of ≈100–200s corresponds rather well to the gel mobility shift experiment. The one-motor model is also in good agreement with the FRET experiment at a low ATP concentration of 2 μM. The nucleosome sliding velocity is computed for different ATP concentrations. The intermediate with equal DNA flanking lengths on either side has the highest probability.

We next considered an extended two-motor model that splits the effective translocation step of the one-motor model into an ATP hydrolysis step with subsequent translocation and an effective kinetic pause during which the remodeler loads a new ATP molecule. A comparison of this two-motor model with the previous effective one-motor model reveals qualitatively similar results for velocity profiles, effective diffusion constants, and probabilities of the intermediates from independent experimental data, i.e., the measured time of the translocation step and the kinetic pause on the one hand and the effective transition rates between intermediates on the other hand. Quantitatively, we obtain only minor intrinsic differences in computed velocity and effective diffusion constants between the two models. Both models are in reasonable agreement with experiments. Therefore, the advanced two-motor model has allowed us to lift the "black box" of the remodeling mechanism employed by ACF a little bit. The description of a detailed communication scheme between the motors and the possible explanation for the phenomenon of kinetic pauses are the benefits of this two-motor model. For the two-motor model to predict center-positioned nucleosomes, the sampling step between the motors is necessary, indicating that the unbinding and binding of ATP molecules at the ATPase unit of either motor are required on top of a simple next ATP binding after the ATP-hydrolysis step. Further remarks and findings confirm that the upper limit of 8/min for the off rate is too high, and a highly processive motor with an off rate of 1/min (or less) improves the agreement with experiments.

While the addition of the motor-loading steps allowed us to make some details of the fueling mechanism of the motors and their synchronization explicit, our model is still simplistic

as far as the mechanics of the motor is concerned. Our next step therefore will be to extend the model by bringing in more mechanistic details of the remodeling mechanism. For this we believe the interaction between modeling and single-molecule experiments to be useful guidance [25]. It should also be kept in mind that due to their inherent complexity and a current lack of sufficiently detailed experiments, in particular only a few low-resolution remodeler structures are available to date [26], only a few theoretical models for a chromatin remodeler function exist so far in the literature [27–31].

ACKNOWLEDGMENT

Y.V. acknowledges support from a postdoctoral contract funded by the CPER Région Nord-Pas de Calais.

[1] C. R. Clapier and B. R. Cairns, Annu. Rev. Biochem. **78**, 273 (2009).
[2] G. D. Bowman, Curr. Opin. Struct. Biol. **20**, 73 (2010).
[3] R. Blossey and H. Schiessel, FEBS J. **278**, 3619 (2011).
[4] W. Dang and B. Bartholomew, Mol. Cell. Biol. **27**, 8306 (2007).
[5] L. R. Racki and G. J. Narlikar, Curr. Opin. Genet. Dev. **18**, 137 (2008).
[6] R. Strohner, M. Wachsmuth, K. Dachauer, J. Mazurkiewicz, J. Hochstatter, K. Rippe, and G. Längst, Nat. Struct. Mol. Biol. **12**, 683 (2005).
[7] B. R. Cairns, Nat. Struct. Mol. Biol. **14**, 989 (2007).
[8] V. K. Gangaraju, P. Prasad, A. Srour, M. N. Kagalwala, and B. Bartholomew, Mol. Cell **35**, 58 (2009).
[9] J. G. Yang, T. S. Madrid, E. Sevastopoulos, and G. J. Narlikar, Nat. Struct. Mol. Biol. **13**, 1078 (2006).
[10] L. R. Racki, J. G. Yang, N. Naber, P. D. Partensky, A. Acevedo, T. J. Purcell, R. Cooke, Y. Cheng, and G. J. Narlikar, Nature (London) **462**, 1016 (2009).
[11] T. R. Blosser, J. G. Yang, M. D. Stone, G. J. Narlikar, and X. Zhuang, Nature (London) **462**, 1022 (2009).
[12] G. J. Narlikar, Curr. Opin. Chem. Biol. **14**, 660 (2010).
[13] A. Saha, J. Wittmeyer, and B. R. Cairns, Nat. Rev. Mol. Cell Biol. **7**, 437 (2006).
[14] F. Erdel, T. Schubert, C. Marth, G. Längst, and K. Rippe, Proc. Natl. Acad. Sci. USA **107**, 19873 (2011).
[15] F. Erdel and K. Rippe, Nucleus **2**, 105 (2011).
[16] R. Blossey and H. Schiessel, HFSP J. **2**, 167 (2008).
[17] R. Blossey and H. Schiessel, Biophys. J. **101**, L30 (2011).
[18] J. J. Hopfield, Proc. Natl. Acad. Sci. USA **71**, 4135 (1974).
[19] U. Alon, *An Introduction to Systems Biology* (CRC, London, 2006).
[20] W. Dang, M. N. Kagalwala, and B. Bartholomew, Mol. Cell. Biol. **26**, 7388 (2006).
[21] E. H. Gerritsma, Ph.D. thesis, Université Libre de Bruxelles, 2010.
[22] Different values of the Michelis constant for experimental ACF systems are found: 11 μM from A. Florescu (private communication) and 50 μM or more from [9].
[23] B. Derrida, J. Stat. Phys. **31**, 433 (1983).
[24] H. Linke, M. T. Downton, and M. J. Zuckermann, Chaos **15**, 26111 (2005); M. E. Fisher and A. B. Kolomeisky, Phys. A **274**, 241 (1999).
[25] G. Lia, M. Inderri, T. Owen-Hughes, L. Finzi, A. Podesta, P. Milani, and D. Dunlap, J. Biophotonics **1**, 280 (2008).
[26] A. E. Leschziner, Curr. Opin. Struct. Biol. **21**, 709 (2011).
[27] T. Chou, Phys. Rev. Lett. **99**, 058105 (2007).
[28] L. Mollazadeh-Beidokhti, F. Mohammad-Rafie, and H. Schiessel, Biophys. J. **96**, 4387 (2009).
[29] V. B. Teif and K. Rippe, Nucleic Acids Res. **37**, 5641 (2009).
[30] A. R. Mazloom, K. Basu, S. S. Mandel, and S. K. Das, BioSystems **99**, 179 (2010).
[31] A. Garai, J. Mani, and D. Chowdhury, Phys. Rev. E **85**, 041902 (2012).